Electro-osmosis of electrorheological fluids

Jayabrata Dhar,[1] Aditya Bandopadhyay,[2] and Suman Chakraborty[1,2,*]
[1]*Department of Mechanical Engineering, Indian Institute of Technology Kharagpur, Kharagpur, India 721302*
[2]*Advanced Technology Development Center, Indian Institute of Technology Kharagpur, Kharagpur, India 721302*
(Received 19 June 2013; published 4 November 2013)

Electrorheological fluids are suspensions that are characterized by a strong functional dependence of the constitutive behavior of the fluids on the electric field. In this work, we consider electro-osmosis of an electrorheological fluid through a channel where a transverse, nonuniform electric field is spontaneously induced due to the presence of an electric double layer that is manifested due to surface charge density at the channel wall. We reveal a nonlinear interplay between the applied electric field, the induced electric field, and the observed flow profiles, which is fundamentally distinctive from other types of nonlinear electrokinetic effects that have been extensively discussed in the literature, in a sense that here an interaction between the applied electric field, the induced electric field, and the dependence of the rheology on the resultant electric field happens to be the focal source of nonlinearity in the observed phenomena. We analyze the electro-osmotic flow control through the exploitation of a combined nonlinear interplay of the driving electrokinetic forces and the resistive viscous interactions, which gives rise to distinctive flow regimes as compared to those realized in cases of either Newtonian fluids or non-Newtonian fluids having electric-field-independent flow rheology.

DOI: 10.1103/PhysRevE.88.053001 PACS number(s): 47.61.−k

I. INTRODUCTION

The alteration in the rheology of materials in the presence of an electric field has been a subject of keen interest in the areas of theoretical and experimental research, with enormous attention paid to a particular kind of fluid, known as electrorheological fluid (ERF) [1–16]. The term electrorheological (ER) effect, also known as the Winslow effect [17], refers to the abrupt change in the apparent viscosity on the application of an electric field. These viscosity variations are very rapid and highly reversible. Owing to the sharp response of rheological alterations to an electric field, one may employ such fluids as smart materials for a wide range of applications [18–22]. Electrorheological fluids are generally nonaqueous suspensions of a noncontinuous phase (nanoparticles or microparticles) dispersed in a nonaqueous phase of continuous media [17,23,24]. Another class of ERF exists wherein only the insulating oil acts as an ERF in the presence of a nonuniform electric field that has been generated by employing electrodes with flocked fabrics [25,26].

In the literature, there exist two kinds of ERFs, namely, the dielectric ERFs and the giant ERFs, which differ in the mechanism and amount of electrorheological effect produced [11,27]. In the present work, we deal with dielectric electrorheological fluids. The fundamental mechanism behind the phenomenological change in rheology of such fluids may be attributed to the polarization of the nanoparticles under an electrostatic field with an effective dipole moment because of the contrast in the dielectric constants between the two phases. As a consequence of the particle dipole-dipole interactions, the particles tend to aggregate and form columnlike structures along the electric-field direction, thus giving rise to field-dependent constitutive behavior [9,27–29].

From a rheological perspective, electrorheological fluids are found to exhibit non-Newtonian features in the presence of an electric field. Rajagopal and Wineman [30] were the pioneers in modeling ER fluids as a continuum medium and formulated a general constitutive relation using the electric field and deformation tensor by employing the Bingham model, to arrive at good agreement with experimental results. Later on, continuum-based models that describe the influence of the orientation of the electric field on ER flow were developed [31]. Several other mathematical formulations were developed in parallel to mathematically model the experimental results for ER flows [32–34].

In all the aforementioned works, the electric field was considered to be dominantly applied in a direction perpendicular to the flow and thus the chaining is observed along the transverse direction of the confinement. In addition, the net electric field is considered to be externally applied and the flow actuation mechanisms considered are either pressure driven or shear driven. However, studies that reveal the interplay of electro-osmotic mechanisms and the electric-field-dependent rheology of ER fluids in narrow confinements are lacking in the literature.

The past couple of decades have witnessed a tremendous development in microfabrication and nanofabrication technologies, which has led to versatile lab on a chip microfluidic and nanofluidic devices [35–38], exploiting the interactions between interfacial electrochemistry and hydrodynamics over small scales. Owing to several advantages such as massive parallelization, ease of miniaturization, and lack of moving parts, development of such devices has led to several applications such as DNA hybridization, power generation, and on-chip assays [39–45]. An important facet of several such devices is flow actuation using electro-osmotic mechanisms [43,46]. Exploiting certain intrinsic characteristics of the electro-osmosis phenomenon, mass flow-rate controllers and their characteristics have been analyzed and studied in the literature of electrokinetics [47,48]. A central concept behind the phenomenon of electro-osmosis is the presence of a net charge density in the medium. Ionic species that have a charge similar to that of the substrate are referred to as coions,

*suman@mech.iitkgp.ernet.in

while those bearing the opposite charge are called counterions. Typically for electrolytes, the distribution of ions away from a charged substrate leads to a higher counterion concentration and decreased coion concentration near the wall. Such a distribution gives rise to the development of an electrically charged layer adjacent to the solid boundary, also known as the electric double layer (EDL) [43]. It may be noted in this context that the substrate may acquire a net charge due to several mechanisms such as selective dissociation on the surface and charge adsorption [45,49–51]. In the presence of the surplus counterions, an electric field applied tangentially to the solid substrate pulls those species, thereby dragging the fluid simultaneously with the species, by viscous action. This phenomenon is known as electro-osmosis, which, for ERFs, may be enriched and complicated by the fact that the viscous force itself is a combined function of the applied tangential electric field as well as the induced transverse electric field, thereby establishing a nonlinear dependence of the flow phenomenon on the electric field. In the present study, we consider a case where only counterions exist in the continuous phase of the ERFs to build up an EDL, thus setting up a transverse field in the flow domain [52,53], which is a consideration fundamentally different from that for combined coion- and counterion-based systems. It is important to mention in this context that ions can also be artificially introduced in the dielectric phase of the ER medium and an external voltage source can induce the nonuniform electric field in the transverse direction [54–56].

Motivated by the concerned intriguing physics as well as a possible plethora of applications, some electrokinetic properties of ERFs in the presence of surfactants have recently been discussed in the literature [57–60]. However, the problem of electro-osmosis of an ER fluid remains unaddressed. A distinctive feature of the transport phenomena of ER fluids under the purview of electro-osmosis, in sharp contrast with the commonly reported ER flows, is that despite no application of a transverse electric field, an induced electric field spontaneously develops here [53,61]. This induced transverse field, coupled with the applied tangential field, affects the flow rheology in a rather intricate manner. In addition, the spontaneously induced transverse electric field also affects the charge distribution in the fluid. The resultant combination of the charge density and the applied electric field interacts with electric-field-dependent resistive (shear) forces in a manner that is intriguingly different from electro-osmotic flows of either Newtonian fluids or non-Newtonian fluids having electric-field-independent flow rheology.

The aim of the present work is to investigate the phenomenon of electro-osmosis of dielectric ERFs, where the transverse electric field is spontaneously induced due to electrochemical mechanisms. Towards this, we first describe the potential and the counterion concentration distribution in the presence of a charge density at the surface of the substrate. In the subsequent analysis, we consider a combination of the transverse electric field (due to the surface charge density) and the applied longitudinal electric field for modeling the constitutive behavior of the ERF as a function of the electric field. In particular, we employ a Bingham-like fluid model, following the considerations of Ceccio and Wineman [31]. The central result of our work is identification of rheology-driven regimes of electro-osmotic flow control through narrow fluidic confinements, which are distinctive from the corresponding regimes established in the presence of Newtonian fluids or non-Newtonian fluids having electric-field-independent flow rheology.

II. MATHEMATICAL DESCRIPTION OF ELECTRO-OSMOTIC FLOW OF AN ELECTRORHEOLOGICAL FLUID

We consider a parallel-plate microfluidic channel (of height $2H$) transmitting an ERF, as schematically depicted in Fig. 1 (the thick dashed line in the figure represents the channel centerline). Only counterions are assumed to be present in the dielectric phase of the electrorheological fluid due to certain electrochemical processes near the wall in the nonaqueous medium [52,53,59,61] while the electroneutrality condition is imposed in the flow domain. Due to the charge distribution, an induced transverse electric field E_2 is spontaneously established, which has a pivotal effect on the flow rheology, apart from an electrokinetic body force generation.

The phenomenon of acquiring a surface charge density by a substrate in the presence of an aqueous electrolyte is considered to be the consequence of a spontaneous electrochemical mechanism [43]. This consideration, however, is highly nonintuitive for cases in which interfaces interact with nonaqueous electrolytic solvents [51]. An interface can acquire a net charge when it comes in contact with another phase (which can be liquid or gas) for many reasons, most common being through the mechanism of charge transfer. Charge separation may occur because of charge transfer across the interface, which predominantly takes place in aqueous media. Nevertheless, other reasons for such occurrence of charge separation exist. These include the presence of surface-active groups in ionizable media and the orientation of permanent or induced dipoles that contribute to the formation of double-layer structures in nonaqueous media [51]. Polar organic solvents such as methanol or acetonitrile contribute to potential drops across the electrode-electrolyte interface. Furthermore, organic electrolytes [52,53] and ionic liquids may induce a typical double layer for some typical electrode-liquid pairs.

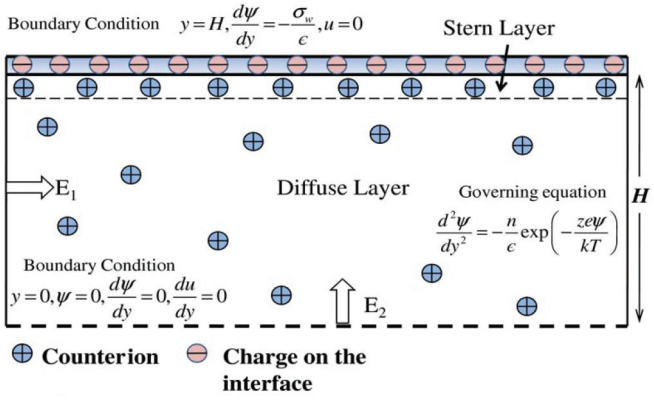

FIG. 1. (Color online) Schematic representation of the flow domain of the ERF contained in a narrow confinement of height $2H$. The thick dotted line represents the channel centerline.

In organic electrolyte capacitors, the interface electrolyte bears a particular charge distribution in which the charge in the wall and that in the diffuse region are opposite to each other. The interfacial charge along with the diffused charge makes up the capacitor [52,53,61]. Such regions are formed due to specific adsorption of charged ionic species of the organic electrolyte even when no potential is applied on an electrode. If a particular organic electrolyte is sandwiched between two interfaces of the same material, then an EDL formation similar to the classical case with two walls having the same charge may be observed. A similar scenario of EDL formation is also found in the case of an ionic liquid-electrode interface wherein the ionic liquid confined between two negatively charged mica sheets induces an EDL structure [59].

Another class of liquids that exhibits the formation of an EDL is liquid crystal in which the charge carriers are the ions. These charge carriers can either be contained in the liquid crystal bulk material or be generated within a liquid crystal by the application of an electric field [62]. The EDL formation when nonaqueous liquid crystals come in contact with the model surface with sufficiently high densities of sodium carboxylate salts has also been studied [63]. Thus one can infer that the EDL structure in nonaqueous media may indeed exist and they have been researched thoroughly in the literature particularly in the context of supercapacitors and fuel cells.

Given the fact that a nonaqueous solvent can induce a surface charge due to certain physicochemical interactions that culminate in the formation of an EDL, we next attempt to address the question of whether these liquids can behave as electrorheological fluids. In essence, an ERF is composed of an organic or aqueous solvent in which a particulate medium (for example, barium titanate oxalate) nanoparticles coated with a very thin layer of urea molecules, in silicone oil [11]) is distributed and the ER effect is exhibited due to the mismatch of effective electrical permittivity between the solute and solvent phase. Such an ER effect has been found in the case of ionic liquids [60]. Even an organic electrolyte can exhibit an ER effect if a particulate phase of different effective electrical permittivity is allowed to disperse in that phase. Furthermore, there have been studies on ERFs in which the solvent phase of the ERF is aqueous [9] or the ER effect is water activated [64,65]. Another class of fluids mentioned above consists of liquid crystals, which also exhibit ER effects [66]. These liquids have an obvious advantage over other classes of ER fluids in that it has a homogeneous structure (does not contain suspended particles) that excludes the possibility of agglomeration or sedimentation and thereby obviates the obstruction of microchannels.

Based on the above considerations, it may be inferred that studying the electrokinetics of ERFs is indeed a scientifically relevant and technologically stimulating proposition. As a first step towards studying the electrokinetics of ERFs, we next investigate the transverse electric potential distribution in the domain.

A. Transverse electric field in the EDL

The potential distribution ψ in the EDL is coupled with the charge density distribution ρ_{el}, which is governed by the Poisson equation, as given by [43,45]

$$\frac{d}{dy}\left(\varepsilon\frac{d\psi}{dy}\right) = -\rho_{el}, \tag{1}$$

where ρ_{el} is the volumetric charge density $\rho_{el} = zen_c$ for the situation where counterions are present only in the solution (with n_c being the number density of counterions that are taken to be positive in this case) and ϵ is the permittivity of the solution. The volumetric charge density in turn is given by the Boltzmann distribution [43,45]

$$\rho_{el} = zen\exp\left(-\frac{ze\psi}{kT}\right). \tag{2}$$

Substitution of Eq. (2) into Eq. (1) leads to

$$\frac{d^2\psi}{dy^2} = -\frac{zen}{\varepsilon}\exp\left(-\frac{ze\psi}{kT}\right). \tag{3}$$

Here e is the protonic charge, z represents the valence of the positively charged species (counterions in this case), T is the absolute temperature, and k is the Boltzmann constant. Here n_b is the unknown bulk number density of counterions and shall be found using the electroneutrality constraint. We solve Eq. (3) subject to the boundary conditions $y = 0$ and $\psi = d\psi/dy = 0$. The solution is given by [67]

$$\psi(y) = \frac{2kT}{ze}\ln\left[\cos\left(\frac{sy}{H}\right)\right]. \tag{4a}$$

A nondimensional form of the EDL potential can be defined as

$$\bar{\phi} = \frac{\psi ze}{kT} = 2\ln[\cos(s\bar{y})], \tag{4b}$$

where the ϵ parameter $s = H(nz^2e^2/2kT\varepsilon)^{1/2}$ is a dimensionless constant, which signifies a dimensionless length on the lines of the penetration layer. Importantly, the bulk number density of ions n cannot be independently specified and must be ascertained consistently with the charge density at the substrate σ_w given by $\sigma_w = -\varepsilon d\psi/dy|_{y=H}$(essentially, an electroneutrality constraint). This in turn implicates that the parameter s is not independent and is evaluated by enforcing the electroneutrality boundary condition given by $s\tan(s) = -(\sigma_w)zeH/2kT\varepsilon$. Typical values of various parameters appearing above are given as follows: $\sigma \sim 10^{-4}\mathrm{C/m^2}$, $H = 10^{-4}$ m, $T \sim 300$ K, $n \sim 1$ mM, and $\varepsilon = 10\varepsilon_0$. The parameter s is analogous to the dimensionless Debye length. However, this being a counterion-only scenario, the Debye screening length is not exactly defined and the double layer virtually penetrates the centerline. Thus the resulting value of the parameter s is of order unity. The electric field that appears due to the nonuniform distribution of the counterions is given by

$$\bar{E}_2(\bar{y}) = -\frac{d\bar{\phi}(\bar{y})}{d\bar{y}} = 2s\tan(s\bar{y}). \tag{5}$$

Having obtained the transverse electric field, we next briefly discuss the functional dependence of the constitutive behavior on the electric field, taking into consideration that the resultant electric field is a combined consequence of the applied tangential electric field E_1 and the induced transverse electric field E_2.

B. Electric-field-dependent rheology: Electrorheological fluid

We first describe the general constitutive behavior of the fluid, following [30]:

$$\begin{aligned}\tau = &-pI + \alpha_1 E\otimes E + \alpha_2 D + \alpha_3 D^2\\ &+\alpha_4(DE\otimes E + E\otimes DE)\\ &+\alpha_5(D^2E\otimes E + E\otimes D^2E).\end{aligned} \tag{6a}$$

Here $\boldsymbol{\tau}$ is the stress tensor, $\mathbf{I}$ is the unitary tensor, $\mathbf{D} = \frac{1}{2}(\mathbf{L}+\mathbf{L}^T)$ is the stretching tensor defined in terms of velocity gradient (with $\mathbf{L} = \boldsymbol{\nabla}\mathbf{u}$), and $\mathbf{E}$ is the electric-field vector. The notation $A\otimes B$ represents the tensor product whose components are given by A_iB_j with respect to the Cartesian coordinates. The scalar p is the indeterminate pressure that arises from the incompressibility criteria of the fluid and the α_i (where $i = 1,2,\ldots,5$) are scalar functions of the set of invariants

$$\begin{aligned}&I_1 = \mathrm{tr}(E\otimes E), \quad I_2 = \mathrm{tr}(D^2), \quad I_3 = \mathrm{tr}(D^3),\\ &I_4 = \mathrm{tr}(DE\otimes E), \quad I_5 = \mathrm{tr}(D^2E\otimes E).\end{aligned} \tag{6b}$$

Equation (6a) for the stress tensor, relating $\boldsymbol{\tau}$, $\mathbf{D}$, and $\mathbf{E}$, is the most general equation and hence includes all physical phenomena that can be predicted in a constitutive equation of this type involving the electric field. The scalar functions α_i are material properties of the fluid that can be determined by experimental work or by employing computer simulations at the microlevel. In essence, Eq. (6) relates the electric-field vector and deformation tensor to the stress tensor in a very generic manner. The above modeling incorporates the observed transient and viscoelastic effects of ER fluids and can predict the solid to fluid transition in response to electric fields. However, a more specific phenomenological relation needs to be adopted for the present scenario, which can properly reflect and predict the rheological behavior that is generally encountered in the pertinent flow conditions.

Towards the above, we first consider a fully developed flow in the x-y plane. The electric-field vector is given by $\mathbf{E} = E_1\mathbf{e}_1 + E_2\mathbf{e}_2$ and the velocity profile is given by $\mathbf{u} = u(x_2)\hat{e}_1$, where $\hat{e}_1$ is directed along x and $\hat{e}_2$ is directed along y. The flow is considered to be incompressible with $\mathrm{tr}(\mathbf{D}) = 0$. The stress tensor [from Eq. (6)] is written as

$$\begin{aligned}\tau_{ij} = &-p\delta_{ij} + \alpha_1 E_iE_j + \alpha_2 D_{ij} + \alpha_3 D_{ik}D_{kj}\\ &+\alpha_4(D_{ik}E_kE_j + E_iD_{jk}E_k)\\ &+\alpha_5(D_{ik}D_{km}E_mE_j + E_iD_{jk}D_{km}E_m),\end{aligned} \tag{6c}$$

where the invariants have the form

$$\begin{aligned}&I_1 = E_iE_i, \quad I_2 = D_{ij}D_{ji}, \quad I_3 = D_{ij}D_{jk}D_{ki},\\ &I_4 = D_{ij}E_jE_i, \quad I_5 = D_{ij}D_{ji}E_iE_j\end{aligned} \tag{6d}$$

and $(i,j)\in(1,2)$. For the present case with the electric-field vector $\mathbf{E} = E_1\mathbf{e}_1 + E_2\mathbf{e}_2$ and velocity vector $\mathbf{u} = u(x_2)\hat{e}_1$, Eq. (6a) reduces to

$$\tau_{11} = -p + \alpha_1E_1^2 + \alpha_4E_1E_2\frac{du}{dy} + \left(\frac{\alpha_3}{4} + \frac{\alpha_5}{2}E_1^2\right)\left(\frac{du}{dy}\right)^2, \tag{7}$$

$$\tau_{22} = -p + \alpha_1E_2^2 + \alpha_4E_1E_2\frac{du}{dy} + \left(\frac{\alpha_3}{4} + \frac{\alpha_5}{2}E_2^2\right)\left(\frac{du}{dy}\right)^2, \tag{8}$$

$$\begin{aligned}\tau_{12} = &\left[\alpha_1 + \frac{\alpha_5}{2}\left(\frac{du}{dy}\right)^2\right]E_1E_2\\ &+\frac{1}{2}\left[\alpha_2 + \alpha_4\left(E_1^2+E_2^2\right)\right]\frac{du}{dy}.\end{aligned} \tag{9a}$$

Let E_0 and θ denote the magnitude of the resultant electric field and its angle with the velocity u, respectively. Then $E_1 = E_0\cos\theta$ and $E_2 = E_0\sin\theta$ and the shear stress tensor has the form

$$\begin{aligned}\tau_{12} = &\frac{1}{4}\left[2\alpha_1 + \alpha_5\left(\frac{du}{dy}\right)^2\right]E_0^2\sin 2\theta\\ &+\frac{1}{2}\left[\alpha_2 + \alpha_4\left(E_0^2\right)\right]\frac{du}{dy},\end{aligned} \tag{9b}$$

where the invariants are given by

$$\begin{aligned}&I_1 = E_0^2, \quad I_2 = \frac{(du/dy)^2}{2}, \quad I_3 = 0,\\ &I_4 = \frac{(du/dy)E_0^2\sin(2\theta)}{2}, \quad I_5 = \frac{(du/dy)^2E_0^2}{4}\end{aligned}$$

and α_i as a function of the invariants has the form

$$\begin{aligned}\alpha_i(I_1,I_2,I_3,I_4,I_5) = \alpha_i\Bigg(&E_0^2, \frac{(du/dy)^2}{2}, 0,\\ &\times\frac{(du/dy)E_0^2\sin(2\theta)}{2}, \frac{(du/dy)^2E_0^2}{4}\Bigg).\end{aligned}$$

Effectively, the shear stress τ_{12} can be rewritten in the reduced form as

$$\tau_{12} = \alpha' E_1E_2 + \mu'\left[E_0^2, \left(\frac{du}{dy}\right)^2\right]\frac{du}{dy}, \tag{9c}$$

where μ' is the effective viscosity, α' is a constant, $E_1 = E_0\cos\theta$, and $E_2 = E_0\sin\theta$.

Investigating Eq. (9b), it is apparent from the first term that an electrorheological body force is induced in the fluid in the longitudinal direction due to the spontaneously induced transverse electric field that suggests that a nonzero shear rate is experienced even when no shear stress is imposed externally. It is also seen that the reversal of flow affects only the invariant I_4 while other invariants remain unaltered, as seen from Eq. (9b). Since the shear stress term τ_{12} is not an odd function of du/dy, τ_{12} is not fully dependent on the direction of the flow. This situation would not have arisen if E_1 were zero. In addition, if the direction of $\mathbf{E}$ is reversed keeping E_0 unaffected while $\theta\to\theta+\pi$, it is seen clearly from Eqs. (9a)–(9c) that the stresses remain unaltered. It has also been seen from various experimental and phenomenological advances that the resistive yield stress for ERFs generally varies as the square of the electric field only [68–71]. Thus a form of Eq. (9c) is chosen that satisfies the limiting condition that in the case when E_1 is zero, the governing equation must be consistent with the constitutive behavior as described by the Bingham model. These considerations are significant in the development of

the modified Bingham equation by Ceccio and Wineman [31], which then appears in the form

$$\tau_{12} = \delta E_0^2 \sin 2\theta + \left[\mu + \frac{\tau_e \hat{B}}{\sqrt{1 + \left(\hat{B}\frac{du}{dy}\right)^2}} \right] \frac{du}{dy}. \quad (10)$$

Here δ and $\hat{B}$ are material constants, μ is the apparent dynamic viscosity, and τ_e is the yield stress for the modified Bingham model fluid and is also assumed to depend on the electric field as $\tau_e = aE_0^2$ [68–70], a being a constant. We have assumed that the apparent viscosity remains constant when there is a component of the electric field along the flow [72]. From Eq. (10) it can be seen that as du/dy increases, the stress term reaches an asymptote $\tau_e + \mu(du/dy)$, which represents the Bingham model. The parameter $\hat{B}$ represents how rapidly the asymptote is reached as du/dy is increased. Physically, the parameter $\hat{B}$ reflects the chaining mechanism in the fluid domain and its influence on the strain rate. The chaining process is governed by the induced polarization within the solute particles and it occurs due to the mismatch in the effective permittivity between the continuous phase and the solute particles. The strength of the columnlike chains formed in the fluid depends on the magnitude of the electric field present. The strength of the structures to resist a shear deformation is quantified through the yield stress, which varies as the square of the magnitude of the electric field. However, the calculated yield stress does not completely obstruct the shearing process since there is a component of the electric field in the flow direction, so the value of $\hat{B}$ determines the fraction of the yield stress that actually, in action, has an adverse effect on the flow. If, however, the value of $\hat{B}$ is kept constant along the transverse region, an increase in the applied field E_1 increases the yield stress, thereby decreasing the velocity, and this gets magnified further as the applied field increases. Further, in practice, an increase in the axial field will have an orientation dominant in the axial direction and thus the flow will experience a reduced obstruction in shear deformation, resulting in a higher velocity. The formulation must reflect this feature through the parameter $\hat{B}$, which varies as E_2/E_1. Referring to the form of $\hat{B}$ [31], we incorporate the variation in $\hat{B}$ as $\hat{B} = B\tan\theta$. This expression takes care of two important limitations. The first is that when the two fields are of similar order, the value of $B = 0.15$ (as used in [31]) remains the same since $\tan\theta \to 1$. Second, when $E_1 \to 0$, $\sqrt{1 + [\hat{B}(du/dy)]^2} \to \hat{B}(du/dy)$; thus the yield stress term tends to τ_e. This reduces the shear stress term $\tau_{12} = \tau_e + \mu(du/dy)$, which represents the classical Bingham model, thus satisfying the above limiting condition.

Next we describe the fluid flow in the x direction, which is governed by the equation (Cauchy-Navier equation) given by [44]

$$0 = \frac{\partial \tau_{11}}{\partial x} + \frac{\partial \tau_{12}}{\partial y} + \rho_{el} E_1. \quad (11)$$

In the absence of an external applied pressure gradient ($\partial p/\partial x = 0$), Eq. (11) reduces to

$$\frac{\partial \tau_{12}}{\partial y} = -\rho_{el} E_1. \quad (12)$$

We then integrate Eq. (12) by imposing the centerline symmetry condition and making use of Eq. (10) to obtain the velocity field as

$$-\varepsilon E_1 E_2 = \delta E_0^2 \sin 2\theta + \left[\mu + \frac{\tau_e \hat{B}}{\sqrt{1 + \left(\hat{B}\frac{du}{dy}\right)^2}} \right] \frac{du}{dy}. \quad (13)$$

Using trigonometric identities it can be shown $\delta E_0^2 \sin 2\theta = 2\delta E_1 E_2$. Therefore, upon substituting $\beta = 2\delta + \varepsilon$, Eq. (13) is recast to form the governing equation as

$$0 = \beta E_1 E_2 + \mu \frac{du}{dy} + \frac{\tau_e \hat{B}}{\sqrt{1 + \left(\hat{B}\frac{du}{dy}\right)^2}} \frac{du}{dy}. \quad (14)$$

Equation (14) is subjected to the no-slip boundary condition at the channel walls. It is also interesting to mention that when $\delta \sim \varepsilon$, the shear developed due to the electrorheological effect in the presence of the two mutually orthogonal fields is of the same order as the shear developed due to the electro-osmotic effects. However, if $\delta \ll \varepsilon$, electro-osmotic forces are more significant over electrorheologically induced shear. For the present study, we assume $\delta \sim \varepsilon$, which is close to the value of δ as chosen by Ciecco and Wineman [31].

It needs to be noted here that the above formulation applies to a steady flow scenario, wherein a postbreakage steady structure of the columns is established. Without any flow-actuating axial electric field, columns are established due to the transverse field and their sizes are comparable to the characteristic length scale of the EDL. However, as a consequence of shear in the flow due to the interaction between the applied axial electric field and the induced transverse electric field, the columnar structures tend to break and attempt to align in the direction of the channel axis. The resultant broken fragments get advected with the flow, whereas the few small stronger columns stick near the electrodes and give rise to the yieldlike property for the ERF. This trend is observed in experimental results [12] as well as simulations on ER fluids [29] with high particle concentration at the electrode walls. In the present scenario, we neglect the initial transients and assume that under a combined action of the axial and transverse electric fields, the columns no longer run from electrode to electrode but are mostly broken due to the flow conditions and are thus quite small in size as compared to the EDL length scale under steady state.

C. Scaling analysis: Three regimes

In this section we identify three scaling regimes for the electro-osmotic flow of electrorheological fluids. We begin with our analysis by first referring to Eq. (14), in which the order magnitude of the first term (term 1) on the right-hand side is $\beta E_1 E_{2m}$, that of the second term (term 2) on the right-hand side is $\mu U/H$, and that of the third term (term 3) on the right-hand side is $BaE_1^2 U/H$, where $E_{2m} = -\sigma_w/\varepsilon$ is the order of magnitude of the maximum transverse electric field and U is the characteristic velocity.

We first consider a case in which the directions of particle chains are predominantly present parallel to the wall of the conduit. As a result, a low magnitude of yield stress occurs that contributes to the flow resistance as opposed to the

viscous resistance of the continuous phase. Mathematically, this corresponds to a low value of the ratio E_{2m}/E_1 at the wall, resulting in a low value of $\tan\theta$. Thus, for the case when the axially applied field is much larger than the transverse electric field, term 1 scales with term 2. Equating the order of both these terms, we arrive at the velocity scale that has the order of magnitude $U_{\mathrm{ref},1} \sim \beta E_1 E_{2m} H/\mu$. Here $U_{\mathrm{ref},1}$ is the velocity scale for the case when $E_1 \gg E_{2m}$, i.e., when the hydrodynamic forces are dominant over the rheological effects due to very low transverse electric field. The velocity scale in this regime resembles the Helmholtz-Smoluchowski velocity scale of electro-osmotic flows of Newtonian fluids.

In the second regime, both the axial and transverse electric fields are of the same order of magnitude $E_{2m} \sim E_1$. Over this regime, the order of magnitude of term 3 is $BaE_1^2 U/H$ as the yield stress has an order of magnitude $\tau_e \sim aE_1^2$ (noting that $E_1 \sim E_2$). In this scaling regime, the yield stress term has a profound effect on the maximum velocity as compared to the viscous effects. In this scenario, term 1 represents the forcing function that drives the flow, whereas the yield stresses, described by term 3, seek to obstruct the shear of the fluid medium. Through this reasoning, term 1 scales with term 3 in this particular case. Equating the order of both of these terms, it is seen that the velocity scales as $U_{\mathrm{ref},2} \sim \beta E_1 E_{2m} H/BaE_1^2$. Here $U_{\mathrm{ref},2}$ represents the velocity scale for the first regime, i.e., $E_{2m} \sim E_1$. For further assessment of the implication of this scenario, we appeal to Eq. (14) with the following nondimensional terms: $\bar{y} = y/H$, $\bar{E}_1 = E_1/E_{\mathrm{ref},1}$, $-d\bar{\phi}/d\bar{y} = E_2/E_{\mathrm{ref},2}$, and $\bar{u} = u/U_{\mathrm{ref}}$. Here the reference transverse electric field $E_{\mathrm{ref},2}$ is taken to be E_{2m}. Writing $\beta = (2\delta+)$, we have the following nondimensional form of Eq. (14):

$$0 = -\bar{E}_1 \frac{d\bar{\phi}}{d\bar{y}} + \frac{\mu}{\eta}\frac{d\bar{u}}{d\bar{y}} + \left[\frac{\tan\theta \frac{d\bar{u}}{d\bar{y}}}{\sqrt{1+\left(\kappa \tan\theta \frac{d\bar{u}}{d\bar{y}}\right)^2}}\left(\bar{E}_1^2 + \left(\frac{E_{2m}^2}{E_{\mathrm{ref},1}^2}\bar{E}_2^2\right)\right)\right],$$

where

$$U_{\mathrm{ref},2} = \frac{H\beta E_{\mathrm{ref},1} E_{2m}}{BaE_{\mathrm{ref},1}^2}.$$

We choose $E_{\mathrm{ref},1} = \varphi/L$ and $E_{2m} = -\sigma_w/\varepsilon$ so that the nondimensional parameters appearing in the above are related as $\mu/\eta = \mu/BaE_{\mathrm{ref},1}^2$ and $\kappa = \beta E_{\mathrm{ref},1} E_{2m}/aE_{\mathrm{ref},1}^2$, with φ being the applied potential across the axial length of the channel and L the length of the channel under consideration. The parametric term μ/η resembles the dimensionless Mason number for electrorheological flows [7,9], which reflects a comparative influence of the hydrodynamic viscous forces on the fluid motion relative to the adverse effect of the yield stress due to the polarization forces on the electro-osmotic flow. Importantly, the modified Bingham model tends to the pure Bingham model as the shear rate increases, as discussed above. The modified Mason number parameter μ/η determines how rapidly μ/η approaches the form of pure Bingham flow model. The parameter κ is effectively the electric driving influence behind fluid flow and is the ratio of the electric actuation force to the critical Bingham yield stress due to the polarization force. This parameter signifies the relative importance of the intrinsic coupling in the electric field, which influences the forcing term as well as the rheological response of the fluid.

A third regime may be identified with the axially applied electric field being much lower than the spontaneously induced transverse field. This is a particular case when the forcing effect on the flow is highly resisted by the high yield stress manifested due to the existence of a relatively strong transverse field and the axial driving force can hardly overcome the effect. However, this effect is felt primarily near the confinement boundary, where the field is comparatively higher because of the high wall charge density and consequently a higher concentration of counterions near the wall. Apart from this region of high interaction between the transverse induced field and the axially applied field, the rest of the fluid is driven mainly by the viscous effect and any change in the liquid viscosity is manifested by a change in the maximum velocity. For the third regime, when $E_{2m} \gg E_1$, two regions based on the particle chain strength and direction can be conceptualized. One region spans near the channel substrate where the yield stress is considerably high due to strong chainlike structure formation attached perpendicular to the wall (characterized by a high shear rate and low flow rate). The onset of bulk flow occurs in the domain in the second region, where the electrokinetic force overcomes the adverse yield stress of the fluid as manifested by the chainlike formation and the particulate chains tend to rearrange towards the shearing direction. Thus, in the region of bulk flow, we conclude that the expression $\hat{B}(du/dy)$ in the denominator of term 3 must be of order unity or less so that the basic flow physics of the ERF remains consistent with the mathematical formulation throughout the flow domain. In other words, the expression $\hat{B}(du/dy)$ should not, anywhere in the domain of flow, be unnecessarily large so that the strain rate term du/dy gets canceled out of term 3, thereby altering the basic form of the equation as developed in [31]. This results in a scenario in which the reference velocity in the bulk is of the order of

$$U_{\mathrm{ref}} \sim \frac{H}{B} \sim \frac{HaE_1^2}{\mu}\frac{\mu}{\eta}.$$

Characteristics of this regime include a low axial electric field (signifying lower force of actuation) and a high induced transverse field (resulting in a strong adverse yield stress effect).

III. RESULTS AND DISCUSSION

The central focus of this work is to highlight the nonlinear interplay of the electric-field-dependent fluid rheology for the electrorheological fluids and the applied electric field. The confluence of these two physical phenomena ranging over the three different scaling regimes is explored to highlight the markedly different physics. In the ensuing analysis we consider physically consistent values from those reported in literature. For illustration we consider an electrorheological fluid having the variation of yield stress as $\tau_e = 87.4E_0^2$ Pa (kV mm^{-2}), while the viscosity is taken as 0.5 Pa s [69,72].

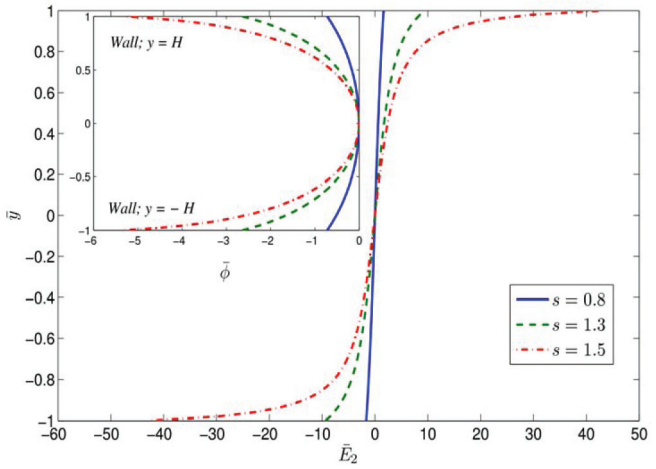

FIG. 2. (Color online) Variation of the induced electric field across the dimensionless channel height for different values of the nondimensional parameter $s = 0.8$, 1.3, and 1.5. The inset depicts the spatial variation of the potential for the parameter s mentioned above.

Before analyzing the electro-osmosis of ERFs, we first study the effect of the surface charge density and the induced transverse electric field. In Fig. 2 we plot the spatial variation of the transverse electric field for different values of the dimensionless characteristic length s. We reiterate the fact that for the case where only counterions are present in the bulk solution, the surface charge density and the dimensionless length are related by the electroneutrality condition given as

$$s\,\tan(s) = \frac{-(\sigma_w)zeH}{2kT\varepsilon}.$$

The inset in Fig. 2 depicts the variation of the potential across the channel due to the charge density at the wall.

A higher value of the parameter s is a direct manifestation of a higher surface charge density. It is observed that for an increase in the value of the dimensionless parameter s, there is an increase in the electric field especially near the walls. From the inset we observe that the potential profile tends to become flatter near the wall as the magnitude of s increases. Thus the strength of the electric field is higher for a high value of the parameter s. For a high wall charge density (or higher s), the counterions exhibit a denser concentration near the wall due to stronger electrostatic interaction. A higher electric field thus leads to a twofold effect on the dynamics of fluid flow, the first being an increase in the electric body force in the longitudinal direction and the second being a local increase in the apparent fluid viscosity that, in the case of ERFs, depends on the electric field. On the contrary, with reduced wall charge densities, the counterions are distributed effectively all across the channel height with a decrease in concentration towards the central axis.

We next obtain a numerical solution for the flow field as governed by Eq. (14). Towards that, we nondimensionalize Eq. (14) using the following parameters:

$$\bar{y} = \frac{y}{H}, \quad \bar{E}_1 = \frac{E_1}{E_{\mathrm{ref},1}}, \quad -\frac{d\bar{\phi}}{d\bar{y}} = \frac{E_2}{E_{\mathrm{ref},2}}, \quad \bar{u} = \frac{u}{U_{\mathrm{ref}}},$$

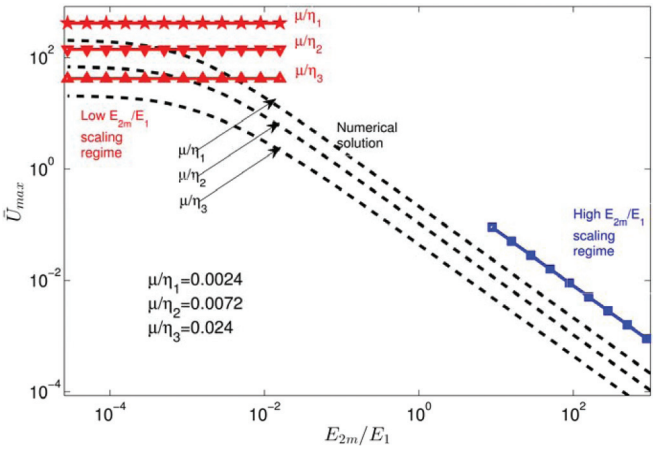

FIG. 3. (Color online) Comparison of the numerical solutions for different modified Mason numbers with the corresponding scaling analysis. Dashed lines represent the data from the numerical solution, whereas the lines with markers represent the scaling predictions.

where

$$U_{\mathrm{ref}} \sim U_{\mathrm{ref},2} = \frac{H\beta E_{\mathrm{ref},1}E_{2m}}{Ba\,E_{\mathrm{ref},1}^2},$$

$$E_{\mathrm{ref},1} = \frac{\varphi}{L},\ E_{\mathrm{ref},2} = E_{2m} \sim \frac{-\sigma_w}{\varepsilon}.$$

It is important to note that all the above-mentioned reference values correspond to the velocity scaling realized over the regime for which $E_1 \sim E_{2m}$. This leads to the following normalized form of Eq. (14):

$$0 = -\bar{E}_1\frac{d\bar{\phi}}{d\bar{y}} + \frac{\mu}{\eta}\frac{d\bar{u}}{d\bar{y}} + \left[\frac{\tan\theta\,\frac{d\bar{u}}{d\bar{y}}}{\sqrt{1+\left(\kappa\tan\theta\,\frac{d\bar{u}}{d\bar{y}}\right)^2}}\left[\bar{E}_1^2 + \left(\frac{E_{2m}^2}{E_{\mathrm{ref},1}^2}\bar{E}_2^2\right)\right]\right].$$

In Fig. 3 the lines plotted without markers represent the numerical solution of the normalized maximum velocity $U_{\max} = u_{\max}/U_{\mathrm{ref},2}$, where $u_{\max}$ is the maximum value of the flow velocity attained for a given value of E_{2m}/E_1. The lines with markers resemble the relative velocity scale of the three scaling regimes. From the figure it is apparent that the numerical solution corroborates the predictions from scaling analysis. From Fig. 3 it is apparent that when $E_{2m} \sim E_1$, $U_{\max} \sim 1$. In contrast, when $E_{2m} \ll E_1$,

$$U_{\max} \sim \frac{U_{\mathrm{ref},1}}{U_{\mathrm{ref},2}} = \frac{Ba\,E_1^2}{\mu},$$

which is in accordance with the scaling predictions described earlier. Analogously, for the regime $E_{2m} \gg E_1$, we have

$$U_{\max} \sim \frac{U_{\mathrm{ref},3}}{U_{\mathrm{ref},2}} = \frac{E_1}{E_{2m}},$$

which corroborates the corresponding scaling predictions as well. The variation of the velocity scales with the modified Mason number parameter μ/η is also depicted in Fig. 3. Notably, over the region $E_{2m} \gg E_1$, the value of $U_{\max}$ turns

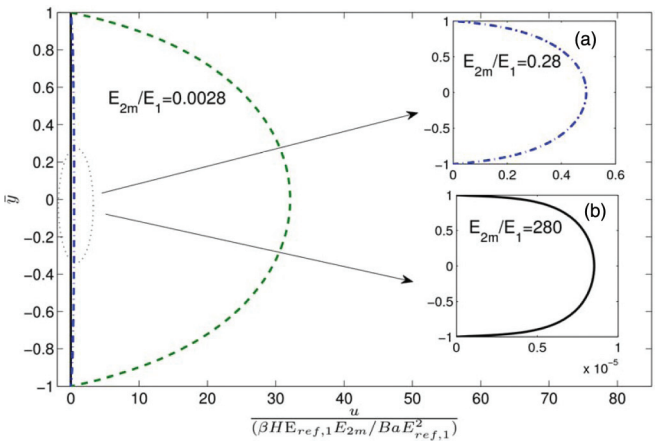

FIG. 4. (Color online) Variation in the nondimensional flow velocity as a function of the nondimensional height for different values of the ratio E_{2m}/E_1 (which also changes the dimensionless parameter κ). The corresponding κ values for increasing E_{2m}/E_1 ratio are $\kappa = 0.0035$, $\kappa = 0.35$, and $\kappa = 350$.

out to be independent of the ratio μ/η, unlike the physical behavior manifested over the other two regimes.

We now proceed to plot the velocity profiles for the three different regimes to highlight that not only does the velocity scale change, but the velocity profile also is significantly altered. In Fig. 4 we plot the velocity profiles for the three cases of $E_1 \sim E_2$, $E_1 \gg E_2$, and $E_1 \ll E_2$.

Figure 4 depicts the variation in the nondimensional flow velocity with nondimensional height for different values of the nondimensional ratio E_{2m}/E_1. An increase in the nondimensional parameter κ implicates the effective dominance of the body force contribution on the actuation of the fluid flow over the yield stress resistance obstructing the flow. Thus the resultant effect on the velocity profiles, due to a combined consequence of the above two influences, is manifested in the increase in flow velocity. In the regime where the induced transverse electric field is much larger than the applied axial electric field, we note that the profile tends to that of a Bingham-like fluid. This feature is dependent on the parameter κ (or, in other words, on the ratio E_{2m}/E_1). Thus, with a high κ value, signifying a higher induced field compared to the applied axial field, a Bingham-like plug profile is obtained, while with a very low value of κ, the profile tends to conform to a Poiseuille-like profile. Further, the nature of the velocity profile for a large value of E_{2m}/E_1 [see Fig. 4(b)] is consistent with the physical interpretation that as the induced field is increased, the yielding resistance increases, which tends to flatten the shape of the velocity profile. In addition, with a high induced transverse electric field, the counterions are concentrated near the confinement boundaries. Accordingly, the rheological variations are largely limited near the wall, inducing an apparent plug flow zone. Unlike Newtonian flows, for the ERFs, there is a nontrivial interplay between the electric body force, the polarization body force, and the adverse yield stress, leading to an intricate physics in the regime where the transverse field has its influence. As a consequence, for a high induced transverse field, the zone where the interplay is realized is restricted to a narrow region near the wall. The rest of the flow is driven solely due to the flow viscosity, thus leading to a pluglike zone. In contrast, with two components of field having similar order $E_{2m} \sim E_1$, the zone where the interplay mentioned above takes place spans the larger depth of the channel, thus leading to a Poiseuille-like profile. Thus this distribution of the electric field plays a pivotal role in dictating the flow behaviors as corroborated by the scaling analysis as well.

IV. CONCLUSION

In order to establish the implications of the nonlinear coupling between electrokinetic transport and electric-field-dependent rheology, we have considered three physically distinct regimes that demarcate the electrorheological fluids from the field-independent non-Newtonian (Bingham) and Newtonian fluids. Through a rigorous mathematical formalism we demonstrate that for a vanishingly small induced transverse electric field (i.e., for very low surface charge density) in the presence of a weak applied field, we observe physical behavior that mimics electro-osmotic transport of Newtonian fluids. We further analyze the case when $E_{2m} \sim E_1$ and capture the difference in the flow profile obtained for that case as compared to that obtained for Newtonian fluids. We also show that when $E_{2m} \gg E_1$, the flow profile tends to have an apparent pluglike shape.

Inferences drawn from the present work may act as valuable pointers towards designing experiments to capture the complex interactions between electrorheology and electro-osmosis. By manipulating the applied and/or induced electric field, one may effectively modulate electro-osmotic transport by exploiting electrorheological phenomena, which can be employed in a wide range of applications such as microfluidic valves and dampers. Exploiting the variations in the flow profile as seen from the three scaling regimes, we may also control the dispersion of neutral species in the flow. A plug profile obtained in the case of a relatively large transverse electric field leads to a lower solute dispersion as compared to the other cases where the profile is nonuniform in nature. By dynamically manipulating the electric fields, one may achieve on-the-fly control of dispersion, which has tremendous potential in lab-on-a-chip applications. Thus electro-osmosis of electrorheological fluid provides exciting prospects for designing futuristic microfluidic and nanofluidic devices with precise and highly maneuverable flow control characteristics.

[1] A. W. Duff, Phys. Rev. **4**, 23 (1896).
[2] T. C. Jordan and M. T. Shaw, IEEE Trans. Electr. Insul. **24**, 849 (1989).
[3] E. N. da C. Andrade and C. Dodd, Proc. R. Soc. London Ser. A **187**, 296 (1946).
[4] T. Hao, A. Kawai, and F. Ikazaki, Langmuir **15**, 918 (1999).

[5] H. P. Schwan and L. D. Sher, J. Electrochem. Soc. **116**, 22C (1969).
[6] J. E. Stangroom, Rev. Phys. Technol. **14**, 290 (1983).
[7] R. S. Allan and S. G. Mason, Proc. R. Soc. London Ser. A **267**, 62 (1962).
[8] H. Ma, W. Wen, W. Y. Tam, and P. Sheng, Phys. Rev. Lett. **77**, 2499 (1996).
[9] M. Parthasarathy and D. Klingenberg, Mater. Sci. Eng. **17**, 57 (1996).
[10] W. Y. Tam, G. H. Yi, W. Wen, H. Ma, M. M. T. Loy, and P. Sheng, Phys. Rev. Lett. **78**, 2987 (1997).
[11] W. Wen, X. Huang, S. Yang, K. Lu, and P. Sheng, Nat. Mater. **2**, 727 (2003).
[12] C. F. Zukoski, Annu. Rev. Mater. Sci. **23**, 45 (1993).
[13] X. Gong, J. Wu, X. Huang, W. Wen, and P. Sheng, Nanotechnology **19**, 165602 (2008).
[14] J. Li, X. Gong, S. Chen, W. Wen, and P. Sheng, J. Appl. Phys. **107**, 093507 (2010).
[15] S. H. Vemuri, M. S. Jhon, K. Zhang, and H. J. Choi, Colloid Polym. Sci. **290**, 189 (2011).
[16] J. Wu, G. Xu, Y. Cheng, F. Liu, J. Guo, and P. Cui, J. Colloid Interface Sci. **378**, 36 (2012).
[17] W. M. Winslow, J. Appl. Phys. **20**, 1137 (1949).
[18] T. Butz and O. von Stryk, ZAMM Z. Angew. Math. Mech. **82**, 3 (2002).
[19] N. D. Sims, R. Stanway, D. J. Peel, W. A. Bullough, and A. R. Johnson, Smart Mater. Struct. **8**, 601 (1999).
[20] D. P. Garg and G. L. Anderson, J. Vib. Control **9**, 1421 (2003).
[21] D. Klein, D. Rensink, H. Freimuth, G. J. Monkman, S. Egersdörfer, H. Böse, and M. Baumann, J. Phys. D **37**, 794 (2004).
[22] R. H. W. Hoppe, W. G. Litvinov, and T. Rahman, SIAM J. Appl. Math. **65**, 1633 (2005).
[23] Y. J. Kim, Y. D. Liu, H. J. Choi, and S.-J. Park, J. Colloid Interface Sci. **394**, 108 (2013).
[24] J. Yin, X. Wang, R. Chang, and X. Zhao, Soft Matter **8**, 294 (2012).
[25] K. Edamura and Y. Otsubo, Rheol. Acta **43**, 180 (2004).
[26] Y. Otsubo and K. Edamura, Rheol. Acta **37**, 500 (1998).
[27] H. See, Korea-Australia Rheol. J. **11**, 169 (1999).
[28] E. C. McIntyre, H. Yang, and P. F. Green, ACS Applied Materials & Interfaces **4**, 2148 (2012).
[29] P. Sheng and W. Wen, Annu. Rev. Fluid Mech. **44**, 143 (2012).
[30] K. R. Rajagopal and A. S. Wineman, Acta Mech. **91**, 57 (1992).
[31] S. L. Ceccio and A. S. Wineman, J. Rheol. **38**, 453 (1994).
[32] K. R. Rajagopal and M. Ružička, Continuum Mech. Thermodyn. **13**, 59 (2001).
[33] W. Eckart and M. Ružička, Int. J. Appl. Mech. Eng. **11**, 813 (2006).
[34] B. Engelmann, R. Hiptmair, R. H. W. Hoppe, and G. Mazurkevitch, Comput. Visual. Sci. **2**, 211 (2000).
[35] H. Daiguji, P. Yang, A. J. Szeri, and A. Majumdar, Nano Lett. **4**, 2315 (2004).
[36] M.-C. Lu, S. Satyanarayana, R. Karnik, A. Majumdar, and C.-C. Wang, J. Micromech. Microeng. **16**, 667 (2006).
[37] F. H. J. van der Heyden, D. J. Bonthuis, D. Stein, C. Meyer, and C. Dekker, Nano Lett. **7**, 1022 (2007).
[38] R. Schoch, J. Han, and P. Renaud, Rev. Mod. Phys. **80**, 839 (2008).
[39] D. Erickson, X. Liu, U. Krull, and D. Li, Anal. Chem. **76**, 7269 (2004).
[40] D. Erickson, D. Li, and U. J. Krull, Anal. Biochem. **317**, 186 (2003).
[41] J. H.-S. Kim, A. Marafie, X.-Y. Jia, J. V. Zoval, and M. J. Madou, Sensor. Actuator. B **113**, 281 (2006).
[42] T. Das, T. K. Maiti, and S. Chakraborty, Integrative Biol. Quant. Biosci. Nano Macro **3**, 684 (2011).
[43] R. J. Hunter, *Zeta Potential in Colloid Science: Principles and Applications* (Academic, London, 1981).
[44] R. F. Probstein, *Physicochemical Hydrodynamics* (Wiley, Hoboken, NJ, 1994).
[45] J. H. Masliyah and S. Bhattacharjee, *Electrokinetic and Colloid Transport Phenomena* (Wiley, Hoboken, NJ, 2006).
[46] S. Chakraborty, Phys. Rev. Lett. **100**, 097801 (2008).
[47] K. Seiler, Z. H. Fan, K. Fluri, and D. J. Harrison, Anal. Chem. **66**, 3485 (1994).
[48] P. Dutta, A. Beskok, and T. C. Warburton, J. Microelectromech. Syst. **11**, 36 (2002).
[49] H. Wright and R. Hunter, Australian J. Chem. **26**, 1191 (1973).
[50] A. A. Hassanali, H. Zhang, C. Knight, Y. K. Shin, and S. J. Singer, J. Chem. Theor. Comput. **6**, 3456 (2010).
[51] S. Srinivasan, *Fuel Cells: From Fundamentals to Applications* (Springer US, Boston, 2006).
[52] I.-T. Kim, M. Egashira, N. Yoshimoto, and M. Morita, Electrochim. Acta **56**, 7319 (2011).
[53] G. Feng, J. Huang, B. G. Sumpter, V. Meunier, and R. Qiao, Phys. Chem. Chem. Phys. **12**, 5468 (2010).
[54] J. R. Harbour and M. L. Hair, J. Phys. Chem. **82**, 1397 (1978).
[55] O. W. Kolling, Trans. Kans. Acad. Sci. **68**, 575 (1965).
[56] J. Li, Y. Wang, H. Lin, and H. Lin, J. Inclus. Phenom. Macrocyclic Chem. **63**, 281 (2008).
[57] H. I. Unal, B. Sahan, and O. Erol, Mater. Chem. Phys. **134**, 382 (2012).
[58] K. Koyuncu, H. I. Unal, O. Y. Gumus, O. Erol, B. Sari, and T. Ergin, Polymer. Adv. Technol. **23**, 1464 (2012).
[59] S. Perkin, L. Crowhurst, H. Niedermeyer, T. Welton, A. M. Smith, and N. N. Gosvami, Chem. Commun. (Cambridge) **47**, 6572 (2011).
[60] M. M. A. Bicak, H. T. Belek, and A. Göksenli, Acta Polytech. **45**, 68 (2005).
[61] D. Jiang, Z. Jin, D. Henderson, and J. Wu, J. Phys. Chem. Lett. **3**, 1727 (2012).
[62] S. Naemura and A. Sawada, Mol. Cryst. Liq. Cryst. **346**, 155 (2000).
[63] R. R. Shah and N. L. Abbott, J. Phys. Chem. B **105**, 4936 (2001).
[64] V. I. Kordonsky, J. Rheol. **35**, 1427 (1991).
[65] H. Uejima, Jpn. J. Appl. Phys. **11**, 319 (1972).
[66] C. I. Mendoza, A. Corella-Madueño, and J. A. Reyes, Phys. Rev. E **77**, 011706 (2008).
[67] S. Engstrom and H. Wennerstrom, J. Phys. Chem. **82**, 2711 (1978).
[68] A. P. Gast and C. F. Zukoski, Adv. Colloid Interface Sci. **30**, 153 (1989).
[69] Y.-Z. Xu, J. Rheol. **35**, 1355 (1991).
[70] T. C. Halsey, Science (NY) **258**, 761 (1992).
[71] W. Wen, X. Huang, and P. Sheng, Soft Matter **4**, 200 (2008).
[72] J. Zhang, X. Gong, C. Liu, W. Wen, and P. Sheng, Phys. Rev. Lett. **101**, 194503 (2008).